Available online at www.sciencedirect.com

ScienceDirect

International Journal of Solids and Structures 44 (2007) 2732–2747

INTERNATIONAL JOURNAL OF SOLIDS and STRUCTURES

www.elsevier.com/locate/ijsolstr

Influence of Vickers tip imperfection on depth sensing indentation tests

J.M. Antunes [a,*], L.F. Menezes [b], J.V. Fernandes [b]

[a] *Escola Superior de Tecnologia de Abrantes, Instituto Politécnico de Tomar, Rua 17 de Agosto de 1808, 2200 Abrantes, Portugal*
[b] *CEMUC, Departamento de Engenharia Mecânica, Faculdade de Ciências e Tecnologia, Polo 2 da Universidade de Coimbra, Pinhal de Marrocos, P-3030-201 Coimbra, Portugal*

Received 26 September 2005; received in revised form 28 June 2006
Available online 22 August 2006

Communicated by D. Hills

Abstract

In the last decade, the development of depth sensing indentation equipment has permitted two of the most conventional mechanical properties of materials to be easily determined: hardness and Young's modulus. Some care is needed to accurate results from the experimental determination of the aforementioned mechanical properties. In this study, numerical simulations were performed on two well-known materials (Bk7 glass, AISI M2 steel) and on fictitious materials with a wide range of mechanical properties, using Vickers indenters with different sizes of tip imperfections. The purpose is to estimate the influence of the size of the defect on the hardness and Young's modulus results obtained by ultramicro and nanoindentation tests.

Keywords: Hardness; Indentation and elastic properties

1. Introduction

The ability of depth sensing indentation equipment to register the load versus the depth indentation, during the test, enables elastic and plastic mechanical properties of the materials to be evaluated. The fact that it is possible to carry out small scale tests of indentation depth makes this technique one of the most powerful tools for the characterization of bulk and thin film materials.

In order to get accurate indentation hardness results, when low load values are used as in ultramicro and nanoindentation, well-defined indenter geometry is required. Nevertheless, it is difficult to obtain an indenter tip with perfect geometry. In the case of the Vickers indenter, the four-sided pyramid typically presents a slight offset near the tip. Experimental procedures have been developed to correct the influence of the tip shape of

* Corresponding author. Tel.: +351 239 790700; fax: +351 239 790701.
E-mail address: jorge.antunes@dem.uc.pt (J.M. Antunes).

0020-7683/$ - see front matter
doi:10.1016/j.ijsolstr.2006.08.017

the Vickers indenter on the hardness and Young's modulus results (see, e.g., Oliver and Pharr, 1992; Trindade et al., 1994; Seitzman, 1998; Herrmann et al., 2000; Antunes et al., 2002; Thurn and Cook, 2002). However, to our knowledge there are no studies concerning the influence of the offset dimension of the Vickers indenter on the hardness and Young's modulus values evaluated by depth sensing indentation, given the natural difficulty of experimentally obtaining different sizes of indenter-offset.

The use of the finite element method in the study of the load–unload indentation curves is an important tool for obtaining greater understanding of the indentation test. The use of this method for the simulation of these kinds of tests allows experimentation with different modulations of indenter geometry, and in particular of the indenter tip. In recent years, many studies have used numerical simulation to describe the indentation process. Most of them use bi-dimensional analyses with spherical and conical indenters (see, e.g., Bhattacharya and Nix, 1988; Laursen and Simo, 1992; Sun et al., 1995; Cai and Bangert, 1995; Bolshakov et al., 1997). There are also studies that present the results of three-dimensional numerical simulations of hardness tests with conical, Vickers and Berkovich indenters (see, e.g., Giannakopoulos et al., 1994; Larsson et al., 1996). However, in all these numerical studies the indenter geometry is modelled perfectly and in most of them no friction between the indenter and the material is taken into account. In a recent study, three-numerical simulations of the hardness test, including friction, were used to perform a preliminary study of the influence of the Vickers offset dimension on the mechanical property results (Antunes et al., 2006). However, the related study only considers the contact area evaluated from the finite element mesh.

This study intends to contribute to a greater understanding of the influence of indenter geometry on contact area determination, when the experimental conditions are reproduced. In this way, a comparison is made between the mechanical property results obtained using two different ways of calculating the contact area of indentation; one directly from the finite element information and the other from the slope of the unloading curve. Different sizes of tip imperfections were studied.

2. Theoretical aspects

The hardness of materials is defined as the ratio between normal force and contact area, defined as follows:

$$H = \frac{P}{A}, \tag{1}$$

where H is the hardness, P is the applied load and A is the contact area of the indentation.

Apart from the hardness, the most important property that can be also evaluated with the hardness tests is the Young's modulus. It can be related to the contact area and the measured unloading compliance, through the expression:

$$E_{\mathrm{R}} = \frac{1}{\beta}\frac{\sqrt{\pi}}{2}\frac{1}{\sqrt{A}}\frac{1}{C}, \tag{2}$$

where β is a correction factor which depends on the geometry of the indenter, A is the contact area and C is the compliance. E_{R} is the reduced Young's modulus, which is a function of the Young's modulus, E, and the Poisson's ratio, v, of the specimen and the indenter (i), through:

$$\frac{1}{E_{\mathrm{R}}} = \frac{1-v^2}{E} + \frac{1-v_i^2}{E_i}. \tag{3}$$

Eq. (2) can be used for axisymmetric and non-axisymmetric indenters, depending on the β value associated with the indenter geometry (Pharr et al., 1992). Using finite element simulations, King (1987) introduced in Eq. (2) the β correction factor for non-axisymmetric indenters. He has proposed several values of β for different indenter geometries (for the Vickers indenter 1.0124, King, 1987). After King (1987) other values of β were found (for Vickers), for example, 1.07 by Dao et al. (2001). A recent study, based on the results obtained from

three-dimensional simulations of the Vickers hardness of several materials with a wide range of mechanical properties (yield stress, strain hardening exponent and Young's modulus) found a correction factor β close to 1.05, slightly dependent on the materials' properties (Antunes et al., 2006).

The methodology used in the compliance evaluation from the unloading curves is an important factor in obtaining precise values for the Young's modulus with Eq. (2). From their experimental results, Oliver and Pharr (1992) observed that the unloading curves are usually well described by a power law in the form:

$$P = K(h - h_f)^m, \tag{4}$$

where P is the load, K and m are constants obtained in the fit to the unload curve, h and h_f are indentation depths at the current value of the load and after unload, respectively. The compliance, C, is obtained by differentiating Eq. (4) with respect to the indentation depth h, at the point of maximum load, resulting in the following equation:

$$\frac{1}{C} = \frac{dP}{dh} = mK(h_{max} - h_f)^{m-1}. \tag{5}$$

The obtained values for the compliance, and consequentially for the Young's modulus values, depend on the fraction of the unload curve fitted by Eq. (4), as has been shown in previous work (Antunes et al., 2006). This study shows that the fraction of the upper part of the unloading curve that must be taken into account in the fit is between 60% and 90%.

As for the hardness calculation, in order to evaluate the Young's modulus a correct definition of the contact area is also needed. Oliver and Pharr (1992) have proposed a method for evaluating the contact area based on the contact indentation depth, h_c, as follows:

$$h_c = h_{max} - \varepsilon P_{max} C, \tag{6}$$

where h_{max} is the indentation depth at the maximum load, P_{max}, C is the compliance and ε is a geometrical parameter that is related to the indenter geometry. This parameter assumes values between 0.72 (conical indenter) and 1 (flat punch) (Sneddon, 1965). Recently, a study of the unload curves, based on the concept of the effective indenter shape, have allowed a more precise definition of the value of the geometrical parameter ε, given by (see, e.g., Oliver and Pharr, 2004):

$$\varepsilon = \left(1 - \frac{2\Gamma\left(\frac{m}{2(m-1)}\right)}{\sqrt{\pi}\Gamma\left(\frac{1}{2(m-1)}\right)}(m-1)\right), \tag{7}$$

where Γ is the factorial or gamma function, and m is the exponent of Eq. (4). The contact area is then calculated as a function of h_c, $A = F(h_c)$, where h_c is evaluated with Eqs. (6) and (7), assuming that the surface of the test material never piles up. When pile-up does appear, it can cause important inaccuracies in the evaluation of the contact area, as in the case of soft materials (low values of H/E) (Antunes et al., 2006).

In addition to the hardness and Young's modulus, another topic of research in the study of the load–unload curves is the potential extraction of the uniaxial mechanical properties, such as, the yield stress and the strain hardening exponent (e.g., Tabor, 1951; Johnson, 1970; Dao et al., 2001; Casals and Alcalá, 2005). Tabor (1951) shows that for ductile materials the hardness, using a Vickers indenter, is proportional to the uniaxial stress, at a representative plastic strain of 0.08, by

$$H = 3.3\sigma_r, \tag{8}$$

where H is the hardness of the material and σ_r is the stress corresponding to the representative plastic strain, ε_r, equal to 0.08. Johnson (1970), shows that the hardness of elastic–plastic materials is governed by the single parameter $(E/\sigma_r)\tan\alpha$, where α is the angle of inclination of the face of the indenter to the surface of the sample, E is the elastic modulus of the material and σ_r is the stress associated to a representative plastic strain, ε_r, which depends on the α angle: $\varepsilon_r = 0.2\tan\alpha$ (Johnson, 1970).

Subsequently, an increasing number of numerical and experimental studies have been conducted in order to achieve a fundamental comprehension of the representative plastic strain and the strain field around the indentations. Recent studies have proposed a representative plastic strain definition, for specific indenter geometry,

which is independent of the strain hardening exponent (see, e.g., Dao et al., 2001; Casals and Alcalá, 2005). Dimensionless functions were proposed to relate the characteristic parameters of indentation load–unloading curves with the mechanical properties obtained from the stress–strain curves. These functions consider that the loading curve can be well described by the following equation, called as Kick's law:

$$P = kh^2, \tag{9}$$

where P is the load, h is the correspondent indentation depth and k is a constant.

The ratio between the constant, k, of Kick's law, and the representative stress, σ_r (k/σ_r), as a function of the ratio between the reduced Young's modulus, E_R, and the representative stress, σ_r (E_R/σ_r), can be used to predict the representative plastic strain, ε_r, for which the following equation (e.g., Dao et al., 2001; Casals and Alcalá, 2005) is independent of the strain hardening coefficient of the stress–strain curve, n:

$$\frac{k}{\sigma_r} = \Pi_1\left(\frac{E_R}{\sigma_r}, n\right), \tag{10}$$

where n is the strain hardening exponent of the stress–plastic strain curve and k is the curvature of the loading curve (Eq. (9)).

In the case of the conical and the Vickers indenters the dimensionless function, Π_1, becomes independent of the strain hardening exponent when the representative stress, σ_r, is associated with a representative plastic strain value, ε_r ($\varepsilon_r = 0.033$ by Dao et al., 2001 and $\varepsilon_r = 0.037$ by Casals and Alcalá, 2005, respectively).

3. Numerical simulation and materials

The numerical simulations were performed using the HAFILM home code. This code was specifically developed to simulate hardness tests with any type of indenter shape taking into account contact with friction between the indenter and the sample. The mechanical model that is the base of the HAFILM code considers the hardness test a quasi-static process that occurs in the domain of large deformation problems. The core of the code was developed in the early nineties and was firstly, and continues to be, applied with success in the simulation of sheet metal forming processes (Menezes et al., 1991; Menezes and Teodosiu, 2000; Oliveira et al., 2003). The development of HAFILM started in 1999 (Antunes et al., 1999; Menezes et al., 2000) and since then the code has been continuously upgraded, today being a freeware virtual laboratory in the field of depth sensing indentation tests.

The plastic behaviour of the material is described by the general yield condition:

$$f(\bar{\sigma}, Y) = \bar{\sigma} - Y = 0. \tag{11}$$

In this equation Y is the flow stress in tension, which is a function of the isotropic strain hardening exponent, described in this study by the Swift equation:

$$Y = C(\varepsilon_0 + \bar{\varepsilon}^p)^n, \tag{12}$$

where C, ε_0 and n are constants for a particular material, determined by classical mechanical tests and $\bar{\varepsilon}^p$ is the equivalent plastic strain. In Eq. (11), $\bar{\sigma}$ is the equivalent stress defined by the plastic yield criterion. In this study the material is assumed to be isotropic and its plastic behaviour is simply described by the Von Mises yield criterion.

One of the most common difficulties in the numerical simulation of the indentation process is related to the time dependence of the boundary conditions due to the contact with friction between the indenter, assumed to be rigid, and the deformable body. In HAFILM the friction contact problem is modelled with a classical Coulomb law. To associate the static equilibrium problem with the friction contact, an augmented Lagrangean method is used in the mechanical formulation. This leads to a system of nonlinear equations, where the cinematic (material displacements) and static variables (contact forces) are the final unknowns of the problem

(Simo and Laursen, 1992). For its resolution the code makes use of a fully implicit algorithm of Newton–Raphson type. All non-linearities, induced by the elastoplastic behaviour of the material and by the friction contact, are treated in a single iterative loop (Menezes and Teodosiu, 2000).

The sample was discretised into isoparametric solid finite elements associated with a selective reduced integration that enables an improvement in the elements to be obtained when large deformations are assumed. Due to the material and geometrical symmetry in the $X = 0$ and $Z = 0$ planes, only a fourth of the sample was used in the numerical simulations (Fig. 1(a)). The finite element mesh was composed of 5832 three-linear eight-node isoparametric hexahedrons. The mesh refinement had previously been optimized, by sensitive studies, in order to guarantee a good estimate of the indentation contact area (Antunes et al., 2006). The number of finite elements in contact with the indenter at the maximum load is given approximately by $N = 240h_{\max} + 16$, where N is the number of finite elements and $h_{\max}$ the maximum indentation depth (excluding the sink-in or pile-up formation). The geometry of the Vickers indenter is modelled with parametric Bézier surfaces allowing an exact description of the indenter tip, namely the contemplation of an indenter tip offset. Five different offset dimensions were considered. Fig. 1(b) shows the Vickers indenters used in the numerical simulation. Table 1 lists the characteristics of the five Vickers indenters.

The real materials used in the numerical simulations were: Bk7 glass, and AISI M2 steel. Table 2 presents the elastic and plastic properties of these two materials. The use of real materials in the simulations allowed a direct comparison with experimental results of the hardness test. In addition, to generalize the analysis, numerical simulations were performed considering a wide range of mechanical properties, namely yield stress, strain hardening and Young's modulus. Table 3 resumes the elastic and plastic properties of these fictitious materials.

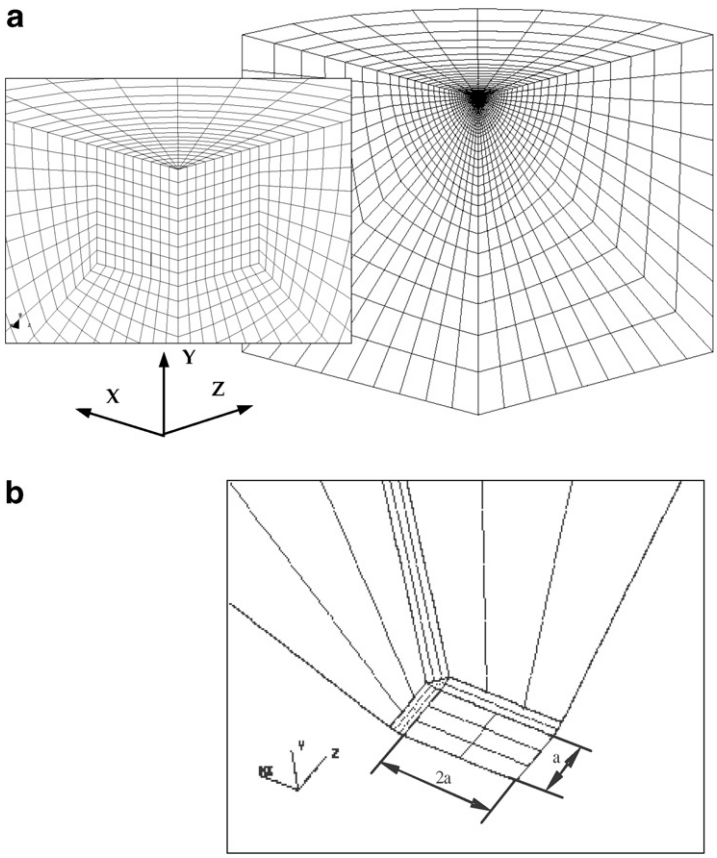

Fig. 1. (a) Finite element mesh used in the numerical simulations and (b) detail of the Vickers indenter tip with offset imperfection.

Table 1
Vickers indenters

Indenter Vickers	a (μm)	Semi-apical angle ($\alpha/2$)	Area function (μm^2)
V1	0.02	68–68.046	$24.561(h+0.008)^2+0.206(h+0.008)$
V2	0.04	68–68.090	$24.615(h+0.016)^2+0.405(h+0.016)$
V3	0.06	68–68.135	$24.671(h+0.024)^2+0.608(h+0.024)$
V4	0.08	68–68.179	$24.727(h+0.032)^2+0.811(h+0.032)$
V5	0.10	68–68.225	$24.784(h+0.040)^2+1.017(h+0.040)$

Table 2
Mechanical properties of the real materials (INDICOAT, 1998)

Material	Y_0 (GPa)	n	E (GPa)	v
Steel AISI M2	4.0	0.010	220	0.290
Bk7	3.5	0.010	82	0.203

Table 3
Mechanical properties of the fictitious materials used in the numerical simulations

Materials	No. studied cases	n	Y_0 (GPa)		E (GPa)	ε_0	v
			Minimum	Maximum			
Without strain hardening	10	≈0	0.25	25	100		
	6	≈0	0.50	60	410		
With strain hardening	6	0.2	0.15	10	100	0.005	0.290
	6	0.4	0.05	6	100		
	10	0.6	0.05	6	100		
	6	0.6	0.15	6	410		

4. Results and discussion

4.1. Friction coefficient

The study of the influence of the friction coefficient on the load–unloading curves was performed for the curves of two real materials (AISI M2 steel and Bk7), using the indenter Vickers V3 (Table 1). In the numerical simulations three values of the friction coefficient were used: 0.08, 0.16 and 0.24. Fig. 2 presents the numerical

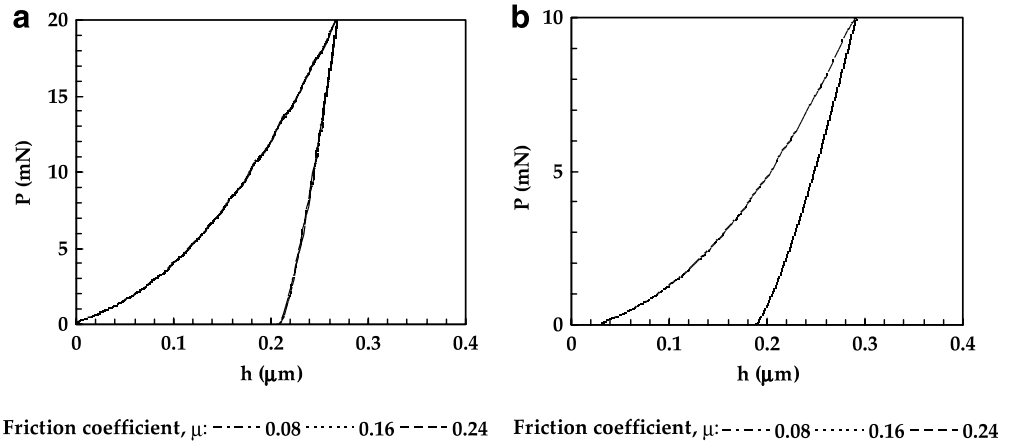

Fig. 2. Load–unload curves obtained in the numerical simulation of the using different friction coefficients, μ: (a) AISI M2 steel and (b) Bk7 glass. The indenter was Vickers V3.

load–unloading curves obtained, using the real mechanical properties of the AISI M2 steel and Bk7 glass, for three values of the friction coefficient: 0.08, 0.16 and 0.24, for each material. The load–unloading curves in Fig. 2 cannot be distinguished, and so they are independent of the friction coefficient value. Moreover, the hardness evaluated for the tested materials slightly depends on the friction coefficient (the difference between maximum and minimum hardness values lower than 5%). Similar conclusions were obtained in a previous study by Antunes et al. (2006).

4.2. Correlations of the indentation results

In order to evaluate the performance of the simulation it is important to make a direct comparison between numerical and experimental results. However, the information in the load–unloading curve is confined to each particular case. So, general information (even if it does not involve load–unloading curves directly) is useful to validate the simulations. Some conditions already tested both experimentally and numerically by other authors (e.g., Johnson, 1970; Dao et al., 2001; Bucaille et al., 2003; Casals and Alcalá, 2005), such as the relationship between the hardness and the Young's modulus, both normalized by so-called representative stress, can be used for validation. This is the basis for the global evaluation which follows. There is also a direct comparison with specific experimental load–unloading curves.

Firstly, the load–unloading curves obtained by numerical simulation and by experimental tests on two real materials were compared. The experimental tests were performed using the FICHERSCOPE ultramicrohardness tester using a Vickers indenter. In the experimental tests a maximum load of 100 mN was applied. In order to minimize the error, several indentation tests were performed on each material. The experimental load–unload curves were compared with the numerical curves obtained using the Vickers indenter V3 (with identical size of the experimental Vickers offset). The mechanical properties of the materials used as input data in the numerical simulation are indicated in Table 2. The friction coefficient was taken to be 0.16 as generally used (Bowden and Tabor, 1950; Lynch, 1980; Antunes et al., 2006). The experimental and the numerical load–unloading curves were corrected with the experimental and numerical indenter area function. Fig. 3 shows the load–unloading curves obtained experimentally and by numerical simulations for the case of the AISI M2 steel and Bk7 glass. There is strong agreement between the loading curves, numerical and experimental. However, the unloading experimental curves present a greater elastic recovery. This fact can be related to the finite stiffness of the experimental equipment and of the diamond indenter. Effectively, the results of the Young's modulus and hardness obtained in the numerical simulation, agree well with the ones evaluated in the experimental tests (differences less then 5% for the hardness and for the Young's modulus). Similar behaviour was previously observed by Ficher-Cripps (2001), in the comparison of experimental and numerical unloading curves obtained from Berkovich hardness tests.

Moreover, the validation of the numerical simulation results was performed using the values of the hardness and the constant k of the loading curve (Eq. (9)) determined in the numerical simulations of the fictitious

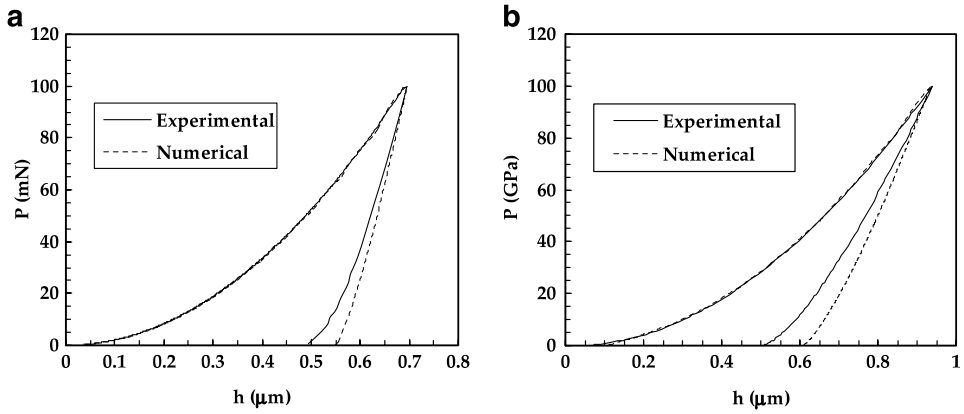

Fig. 3. Comparison between the experimental and the numerical load–unload curves: (a) AISI M2 steel and (b) Bk7 glass.

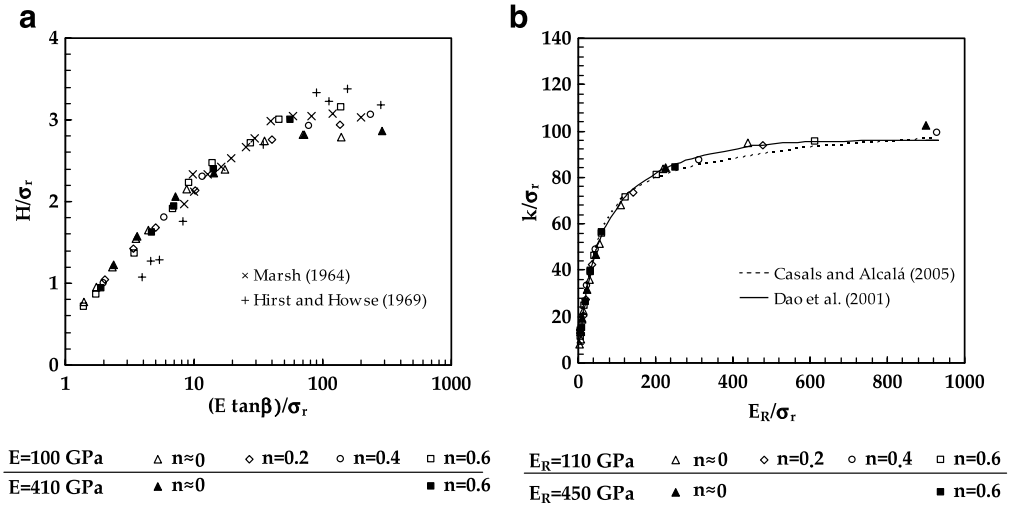

Fig. 4. Correlation of experiments with Vickers indenter: (a) representative strain equal to 0.07 and (b) representative strain equal to 0.037.

materials (Table 3). For this purpose the values of the characteristic stress, σ_r, and an associated representative strain, ε_r, equal to 0.07 (Johnson, 1970) and 0.037 (Casals and Alcalá, 2005), were considered for the case of the Vickers indenter. Fig. 4(a) shows the representation of the ratio between hardness and characteristic stress, H/σ_r, as function of the ratio between Young's modulus and characteristic stress, E_R/σ_r, for the fictitious materials of Table 3 ($\varepsilon_r = 0.07$, Johnson, 1970). Fig. 4(a) also shows, for comparison, the evolution obtained from two different experimental studies with a Vickers indenter (Marsh, 1964; Hirst and Howse, 1969). Fig. 4(b) presents the evolution of the ratio k/σ_r ($\varepsilon_r = 0.037$, Casals and Alcalá, 2005) as function of the ratio E_R/σ_r, for the materials of Table 3. The evolution predicted by Dao et al. (2001) is also shown in this figure, considering $\varepsilon_r = 0.033$ for a conical indenter with an apical angle equal to 70.3°.

Fig. 4(a) shows that the evolution obtained for the materials with different mechanical properties is independent of the representative plastic strain (0.07), for values of the ratio of $H/\sigma_r \leqslant 2.8$. For superior values the evolution depends on the strain hardening exponent of the materials. The results in Fig. 4(a) show agreement

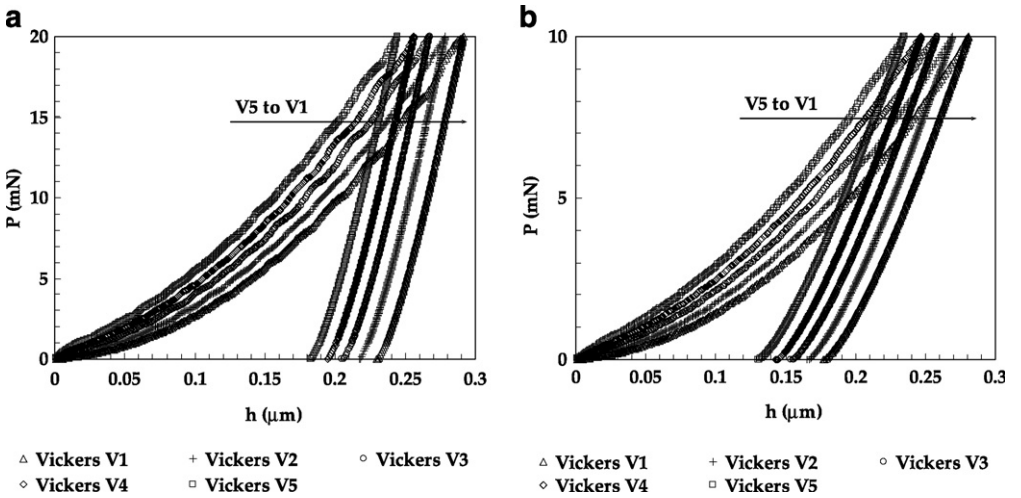

Fig. 5. Numerical load–unload curves as obtained (without offset correction), for the two real materials: (a) AISI M2 steel and (b) Bk7 glass.

with the ones previously obtained during the experimental indentation of various materials with a Vickers indenter by Marsh (1964) and Hirst and Howse (1969). Where the representative plastic strain considered was 0.037, Fig. 4(b), the representation is independent of the strain hardening exponent. In addition, the results in Fig. 4(b) also correspond to the evolutions predicted by Dao et al. (2001), in the numerical simulation of different materials with a conical indenter (apical angle equal to 70.3°) without friction.

4.3. Load–unload curves, strain distribution and indentation geometry

Fig. 5 presents the load–unloading curves obtained by numerical simulations with the five different Vickers indenters for the two real materials (AISI M2 steel and Bk7 glass). The results show that indentation depth increases as the size of the indenter-offset decreases, for the same load value. Fig. 6 presents the same curves as Fig. 5, but has been corrected, taking into account the area function of each indenter. In these figures, h_{AF} corresponds to the indentation depth obtained with an ideal indenter, without defects: $h_{AF} = \sqrt{A/24.5}$ (for the area function A, see Table 1). The curves become almost coincident after correction. This indicates that the

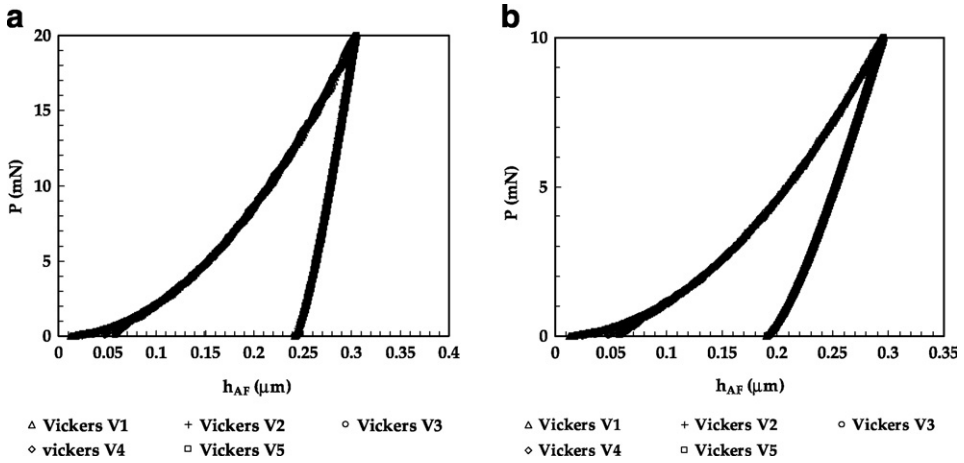

Fig. 6. Numerical load–unload curves obtained for the two materials with offset correction, using the area function of each indenter: (a) AISI M2 steel and (b) Bk7 glass.

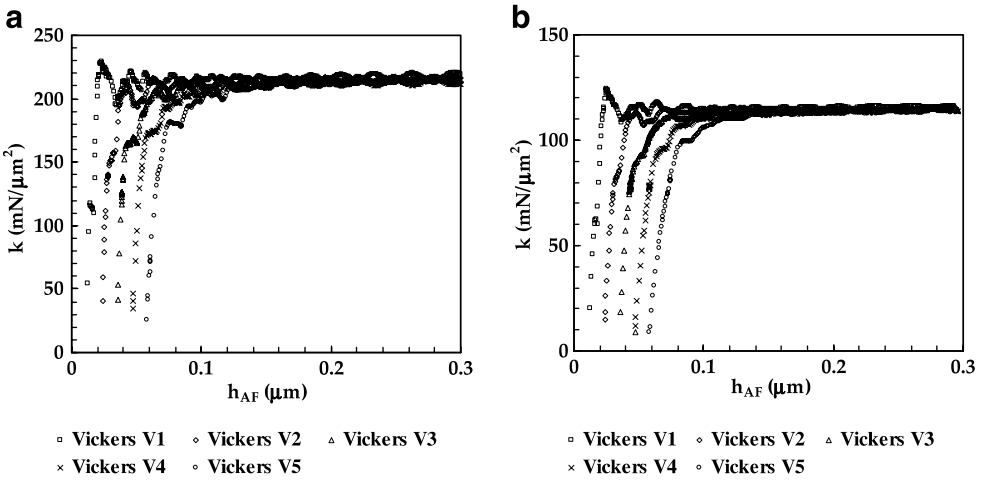

Fig. 7. Evolution of the value of the constant k as function of the indentation depth, obtained in the numerical simulation with the five Vickers indenters: (a) AISI M2 steel and (b) Bk7 glass.

correction of the geometry of the indenters with offset, using the respective area function, seems to be enough to obtain the mechanical properties, namely the Young's modulus and the hardness.

In order to ensure that the correction with the area function of the load–unloading curves is sufficient, the evolution of $k = P/h^2$ (from Eq. (9)), at each loading point, was represented as function of the indentation depth, for the different offset sizes. This representation is presented in Fig. 7 for the case of the AISI M2 steel and Bk7 glass. Fig. 7 shows that, for indentation depths higher than 0.15 μm, the $k = P/h^2$ becomes constant and is independent of the offset dimension. This means that the loading curves are self similar after this indentation depth.

Figs. 8 and 9 show the distributions of the equivalent plastic strain obtained for the Bk7 glass in the numerical simulation of the Vickers V1 and V5 indenters, respectively, for indentations depths of: 0.1, 0.2, 0.3, 0.4 and 0.5 μm. These figures show that the maximum value of equivalent plastic strain only slightly depends on the value of maximum indentation depth once the indentation depth values are greater than 0.3 μm. However, the distributions of the equivalent plastic strain obtained with the Vickers V5 indenter presents maximum

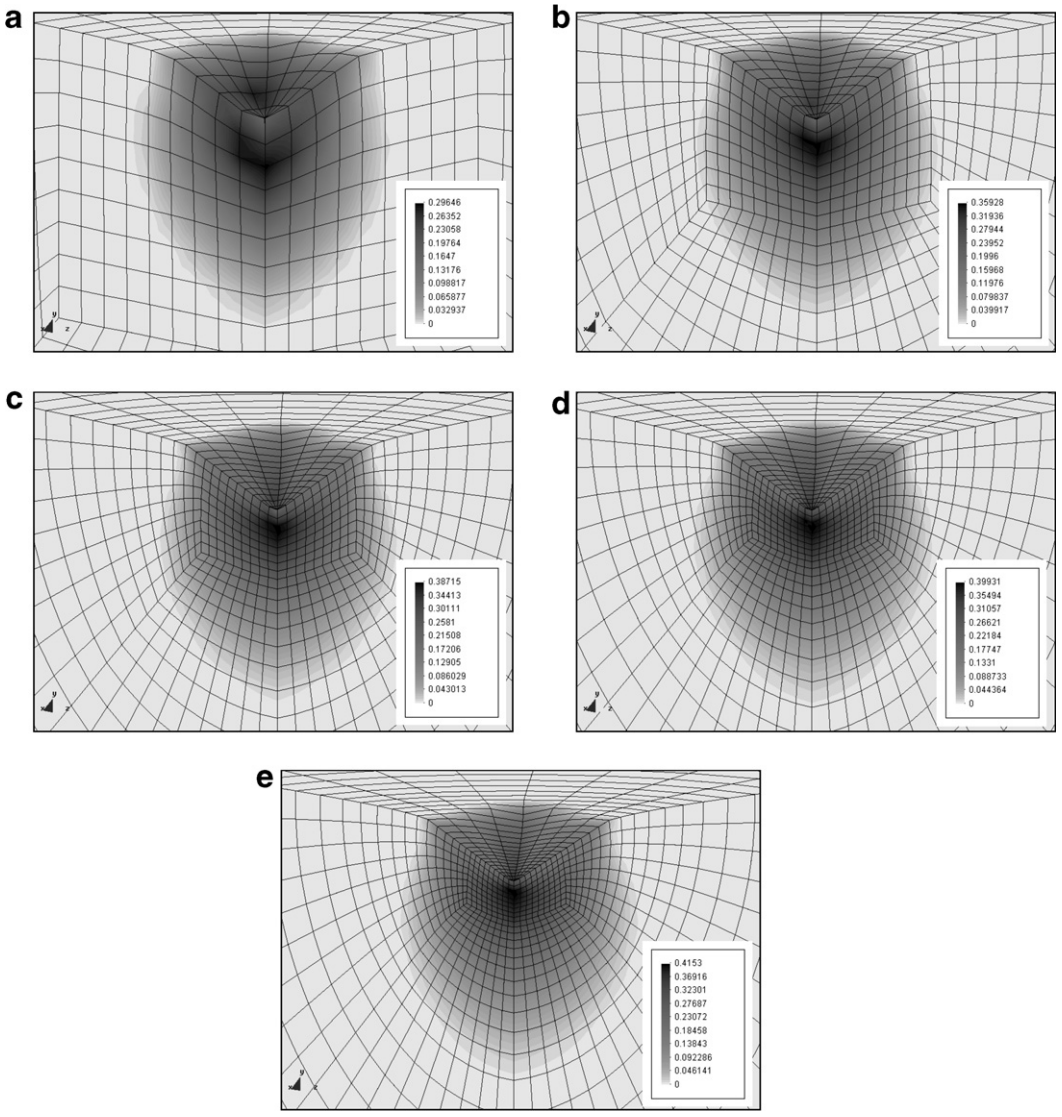

Fig. 8. Finite element mesh showing equivalent plastic strain distribution obtained, at different indentation depths, in the numerical simulations of the Bk7 glass with the indenter Vickers V1: (a) $h = 0.1$ μm; (b) $h = 0.2$ μm; (c) $h = 0.3$ μm; (d) $h = 0.4$ μm; (e) $h = 0.5$ μm.

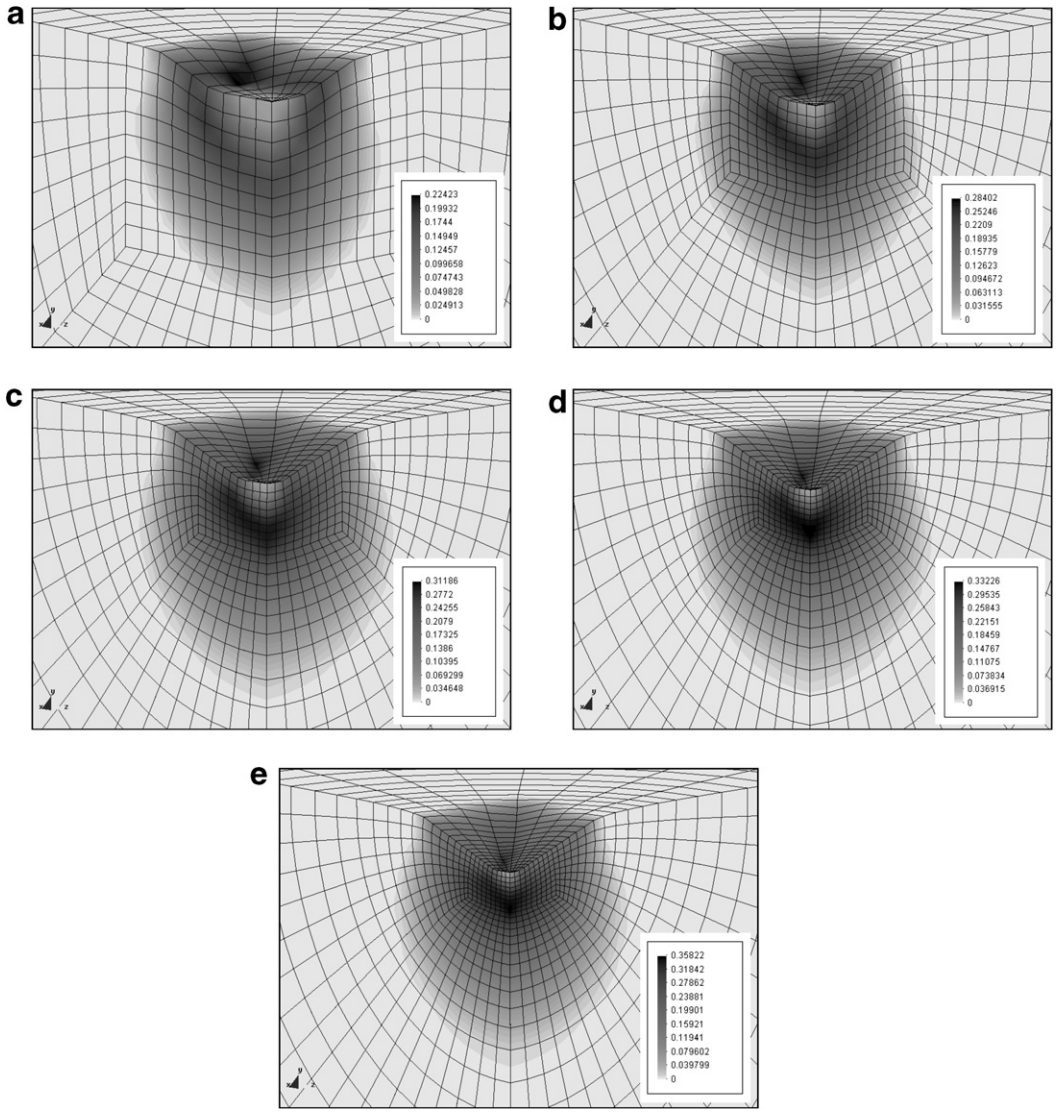

Fig. 9. As Fig. 8 but for the indenter Vickers V5: (a) $h = 0.1$ μm; (b) $h = 0.2$ μm; (c) $h = 0.3$ μm; (d) $h = 0.4$ μm; (e) $h = 0.5$ μm.

values lower than the ones attained with the Vickers V1 indenter. Moreover, in the case of the Vickers V5 indentations, the distributions show that under the centre of the offset region, the deformation is almost zero when the size of the offset becomes higher (Fig. 9). This may be caused by the presence of a hydrostatic stress state in this region, which increases with the increasing value of the offset.

In conclusion, the distributions of equivalent plastic strain are similar and independent of the offset size, for indentation depths higher than 0.3 μm. Only the maximum plastic strain values depend on the offset dimension.

4.4. Young's modulus

For the five indenter offsets tested, the Young's modulus of the various fictitious materials was evaluated from the load–unload curves, following the considerations described above, and using Eqs. (2) and (3). In Eq. (2) the term C, represents the compliance at the beginning of the unloading curve; these values were

determined by fitting 70% of the unloading curve to an equation of the type of Eq. (5) as follows (Antunes et al., 2006):

$$P = P_0 + T(h - h_0)^q, \tag{13}$$

where P_0 is the lower load considered in the fit of the unloading curve, which corresponds to the indentation depth h_0. T and q are the fitted constants. The compliance, C of Eq. (2), was calculated using the curves after correction with the area function.

Two different values of Young's modulus, E_{FE} and E_{hc}, were evaluated for each indenter and material. E_{FE} is calculated considering the indentation contact area A_{FE}, which is evaluated with the contour of the nodes of the finite element mesh in contact with the indenter at the maximum load. E_{hc} is calculated considering the contact area A_{hc}, which is obtained from the indention contact depth h_c, Eqs. (6) and (7), as performed experimentally. In Eq. (2) a correction factor β equal to 1.05 was used in the evaluation of the Young's modulus, as was discussed in a previous study (Antunes et al., 2006).

The five indenters were used to simulate hardness tests, up to a maximum indentation depth close to 0.3 μm, on sets of five different materials, having strain hardening values of, $n \approx 0$, 0.2, 0.4 and 0.6 and Young's modulus, E, equal to 100 and 410 GPa. In each set, five different values of the ratio h_f/h_{max} were considered (from at about 0.13 to 0.97), which corresponds to different values of the ratio of hardness to Young's modulus (Bolshakov et al., 1997). Table 3 summarizes the mechanical properties of these materials.

Fig. 10 presents the calculated Young's modulus, E_{FE} and E_{hc} normalized by the input value E_{Input} as a function of h_f/h_{max}, for the materials with Young's modulus equal to 100 GPa (as shown below) this relation-

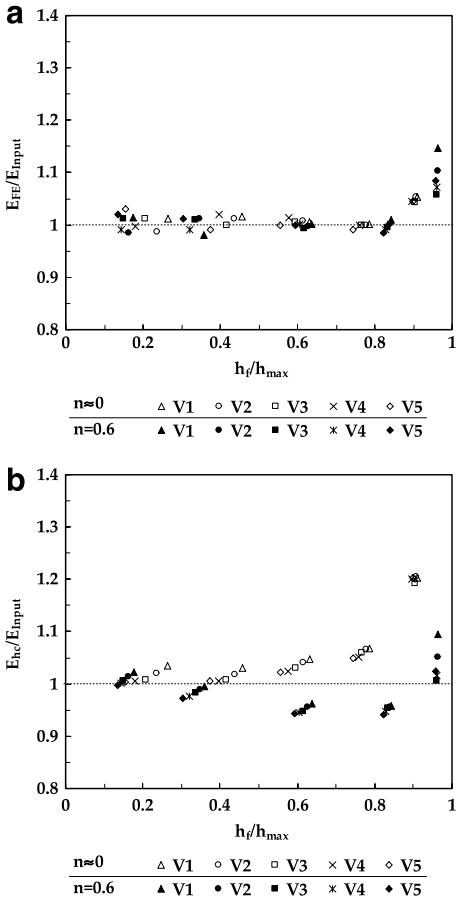

Fig. 10. Normalized Young's modulus numerical results obtained with the five Vickers indenters, for the fictitious materials with a Young's modulus equal to 100 GPa: (a) E_{FE}/E_{Input}, obtained with the contact area A_{FE}. (b) E_{hc}/E_{Input} obtained with the contact area A_{hc}.

ship does not depend on the Young's modulus value. The Young's modulus values E_{FE}/E_{Input} presented in Fig. 10(a) depend neither on the strain hardening exponent nor the offset dimension of the indenter. As previously discussed (Antunes et al., 2006), for a given offset size (Vickers V3 indenter), the β value of 1.05 used in Eq. (2) is well chosen, except for values of h_f/h_{max} in the range 0.90–1. The over evaluation of the Young' modulus when h_f/h_{max} is close to 1, mainly in non-strain hardening materials, is related to pile-up formation (Antunes et al., 2006; Bolshakov et al., 1997). Moreover, the results shown in Fig. 10(a) demonstrate that, for the other cases, the β value does not depend on the size of the indenter-offset.

The results concerned with the values of E_{hc}/E_{Input}, calculated using the contact area obtained as if by experimentation from the unloading curve, show dependence on the strain hardening exponent, as shown in Fig. 10(b). Moreover, they show little dependence on the size of the indenter-offset. So, from an experimental point of view, it is acceptable to correct the experimental curve using the area function of the indenter, the experimental results obtained are quite acceptable: in just two cases studied is the error higher than at about 6% (Fig. 10(b)). Also, for experimental determination of mechanical properties using such a Vickers indenter-offset, the use of a value of the β value equal to 1.05 is adequate. As mentioned above, Fig. 10(a) shows that (except for the two highest values of h_f/h_{max}, close to 1) the Young's modulus is quite accurately calculated when the genuine contact area A_{FE}, evaluated from the contour of the nodes of the finite element mesh in contact with the indenter, is used in Eq. (2). This means that the corresponding compliance values necessary to enter in Eq. (2) are correctly evaluated from the slope of the unloading curve at the maximum load. Taking into account that the compliance does not depend on the way used to evaluate the contact areas, A_{FE} or A_{hc}, the values of A_{hc} must be slightly inaccurate, because the correction of the loading curves, which uses the

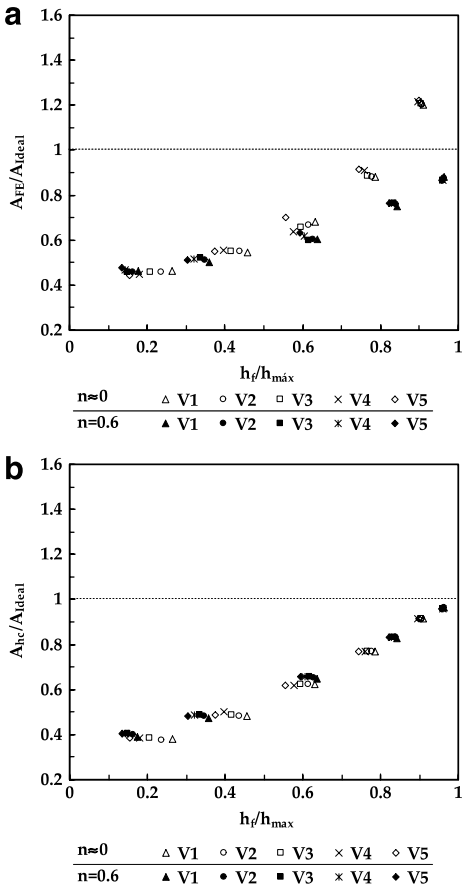

Fig. 11. Normalized contact area results obtained with the five Vickers indenters, for the fictitious materials: (a) A_{FE}/A_{AF} and (b) A_{hc}/A_{AF}.

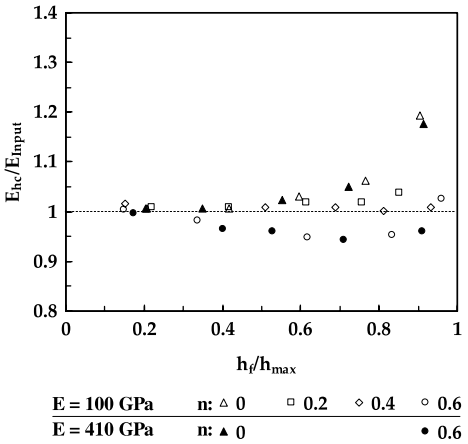

Fig. 12. Normalized Young's modulus numerical results E_{hc}/E_{Input}, obtained with the Vickers indenter V3, in fictitious materials with strain hardening, $n = 0$ and $n = 0.6$, for two cases of Young's modulus, $E = 100$ and 410 GPa.

indenter area function, is not performed in a satisfactory way. A fact illustrated by the corrected curves shown in Fig. 6, which are not entirely coincident.

In this context, we present in Fig. 11 the indentation contact area, A_{FE} and A_{hc} normalized by the indenter area function A_{Ideal} (A_{Ideal} is the projected reference area, obtained when the indentation geometry does not present pile-up or sink-in formation) as a function of h_f/h_{max}. The contact area values A_{FE}/A_{Ideal} presented in Fig. 12(a) depend only slightly on the offset dimension, for each case of work-hardening coefficient. For the case of the materials without strain hardening ($n = 0$), the normalized contact area is greater than 1 for the values of the ratio h_f/h_{max} higher than 0.8. When the material presents high values of work-hardening ($n = 0.6$), the contact area is less than 1, for all values of h_f/h_{max}. The contact area values A_{hc}/A_{Ideal}, presented in Fig. 11(b), are rather independent of the work-hardening coefficient. The normalized contact area is less than 1 in the whole range of h_f/h_{max}.

Therefore, it can be concluded that the accurate evaluation of the Young's modulus using the contact area, A_{hc}, as usually done experimentally, depends only slightly on the size of the indenter-offset. In addition, the eventual experimental correction of the contact area, A_{hc}, and consequently of the mechanical properties depends on the work-hardening coefficient and on the ratio h_f/h_{max}, as can be seen in Fig. 10(b).

The influence of the Young's modulus and the work-hardening coefficient on the determination of mechanical properties was also tested. Two values of the Young's modulus ($E = 100$ and 410 GPa) and four values of strain hardening exponent ($n = 0$, 0.2, 0.4 and 0.6, for the case of $E = 100$ GPa) were used in this study (Table 3). The results of the normalized Young's modulus E_{hc}/E_{Input}, were obtained in numerical simulations with the indenter Vickers V3. Fig. 12 shows that the ratio E_{hc}/E_{Input} remains close to 1 ($\pm 6\%$), except for the case of the materials with the lowest values of strain hardening exponent (n close to zero) when h_f/h_{max} becomes close to 1. For the materials with strain hardening exponents of 0 and 0.6, the results of the normalized Young's modulus do not present dependence on the Young's modulus value (100 and 410 GPa, respectively).

5. Conclusions

The evaluation of mechanical properties, namely the Young's modulus and hardness, by using ultramicro or nanoindentation tests, must take into account the fact that the experimental indenter geometry is not ideal.

In this study, a numerical simulation of the hardness test was used to study the influence of the presence and size of the most common imprecision in Vickers geometry, designated as offset. The modulation of the indenter was performed for five different sizes of offset. Materials with different mechanical properties, namely hardness, strain hardening exponent and Young's modulus, were used in this investigation. The main conclusions of this study, concerning real and fictitious materials, are as follows:

(a) The comparison between the experimental and the numerical load–unload curves shows strong agreement. However, the experimental unloading curves present a greater elastic recovery, a fact justified by the finite stiffness of the experimental equipment and of the diamond indenter. Also, the load–unload curves are independent of the friction coefficient.
(b) When the contact area is evaluated from the contour of the nodes of the finite element method, the Young's modulus can be accurately evaluated when a correction factor β equal to 1.05 is used, whatever the size of the indenter-offset and the material tested. However, the presence of strong pile-up on the surface of the material can introduce an error in the prediction of the mechanical property, for h_f/h_{max} higher than at about 0.90, for which the Young's modulus can be overestimated.
(c) For the general case of calculation of the mechanical properties from A_{hc}, evaluated from the slope of the unloading curve, as if experimentally, the use of the area function of the indenter for correcting the load–unloading curves gives rise to slightly greater errors (within the range of $\pm 6\%$, in most cases; for h_f/h_{max} higher than at about 0.9, the Young's modulus can be overestimated) than when calculated from A_{FE}. These results are nevertheless acceptable, but further correction of the contact area, considering the indentation surface geometry, is needed in order to obtain more accurate mechanical properties. The results depend on the strain hardening exponent of the materials and on the ratio h_f/h_{max} (or H/E), but not on the value of the Young's modulus. These results were also obtained for a correction factor β equal to 1.05.

Acknowledgements

The authors are grateful to the Portuguese Foundation for Science and Technology (FCT) who financially supported this work, through the Program POCTI (Portuguese Government and FEDER).

References

Antunes, J.M., Menezes, L.F., Fernandes, J.V., 1999. Three-dimensional numerical simulation of tensile tests in coatings. In: Covas, J.A. (Ed.), Proceedings of the Second Esaform Conference on Metal Forming, Guimarães, pp. 159–162.

Antunes, J.M., Cavaleiro, A., Menezes, L.F., Simões, M.I., Fernandes, J.V., 2002. Ultra-microhardness testing procedure with Vickers indenter. Surface & Coatings Technology 149 (1), 27–35.

Antunes, J.M., Menezes, L.F., Fernandes, J.V., 2006. Three-dimensional numerical simulation of Vickers indentation tests. International Journal of Solids and Structures 43 (3–4), 784–806.

Bhattacharya, A.K., Nix, W.D., 1988. Finite element simulation of indentation experiments. International Journal of Solids and Structures 24 (9), 881–891.

Bolshakov, A., Oliver, W.C., Pharr, G.M., 1997. Finite element studies of the influence of pile-up on the analysis of nanoindentation data. In: Materials Research Society Symposium 436, p. 141.

Bowden, F.P., Tabor, D., 1950The Friction and Lubrication in Solids, vol. 1. Clarendon Press.

Bucaille, J.L., Strauss, S., Felder, E., Michler, J., 2003. Determination of plastic properties of metals by instrumented indentation using different sharp indenters. Acta Materialia 51 (6), 1663–1678.

Cai, X., Bangert, H., 1995. Hardness measurements of thin films-determining the critical ratio of depth to thickness using FEM. Thin Solid Films 264 (1), 59–71.

Casals, O., Alcalá, J., 2005. The duality in mechanical property extractions from Vickers and Berkovich instrumented indentation experiments. Acta Materialia 53 (13), 3545–3561.

Dao, M., Chollacoop, N., Van Vliet, K.J., Venkatesh, T.A., Suresh, S., 2001. Computational modelling of the forward reverse problems in instrumented sharp indentation. Acta Materialia 49 (19), 3899–3918.

Ficher-Cripps, A.C., 2001. Simulation of sub-micron indentation tests with spherical and Berkovich indenters. Journal of Materials Research 16 (7), 2149.

Giannakopoulos, A.E., Larson, P-L., Soderlund, E., Rowcliffe, D.J., Vestergaard, R., 1994. Analysis of Vickers indentation. International Journal of Solids and Structures 31 (19), 2679–2708.

Herrmann, K., Jennett, N.M., Wegener, W., Meneve, J., Hasche, K., Seemann, R., 2000. Progress in determination of the area function of indenters used for nanoindentation. Thin Solid Films 377 (1), 394–400.

Hirst, W., Howse, M.G.J.W., 1969. Indentation of materials by wedges. Proceedings of the Royal Society of London Series A – Mathematical and Physical Sciences 311 (1506), 429.

INDICOAT, 1998. European Commission – Standards, Measurements and Testing Programme (SMT). Determination of Hardness and Modulus of Thin Films and Coatings by Nanoindentation – INDICOAT Contract SMT4 – CT98/2249.

Johnson, K.L., 1970. Correlation of indentation experiments. Journal of the Mechanics and Physics of Solids 18 (2), 115.

King, R.B., 1987. Elastic analysis of some punch problems for a layered medium. International Journal of Solids and Structures 23 (12), 1657–1664.

Larsson, P-L., Giannakopoulos, A.E., Vestergaard, R., 1996. Analysis of Berkovich indentation. International Journal of Solids Structures 33 (2), 221–248.

Laursen, T.A., Simo, J.C., 1992. A study of the mechanics of microindentation using finite-elements. Journal of Materials Research 7 (3), 618–626.

Lynch, C.T., 1980. Handbook of Materials Science, Volume 1: General Properties. CRC Press.

Marsh, D.M., 1964. Plastic flow in glass. Proceedings of the Royal Society of London Series A – Mathematical and Physical Sciences 279 (137), 420.

Menezes, L.F., Teodosiu, C., 2000. Three-dimensional numerical simulation of the deep-drawing process using solid finite elements. Journal of Materials Processing Technology 97 (1-3), 100–106.

Menezes, L.F., Teodosiu, C., Makinouchi, A., 1991. A 3-D solid elasto-plastic elements for simulating sheet metal forming processes by the finite element method. In: FE-Simulation of 3-D Sheet Metal Forming Processes in Automotive IndustryTagungshericht der VDI-Gesellschaft Fahrzeugtechnik, vol. 894. VDI VERLAG, Dusseldorf, pp. 381–403.

Menezes, L.F., Fernandes, J.V., Trindade, A., 2000. Numerical simulation of hardness tests. In: Fritz, H.-G. (Ed.), Proceedings of the 3rd ESAFORM Conference on Material Forming, Stuttgart, Universitat Stuttgart, pp. VII.19–VII.22.

Oliveira, M.C., Alves, J.L., Menezes, L.F., 2003. Improvement of a frictional contact algorithm for a strongly curved contact problems. International Journal for Numerical Methods in Engineering 58 (14), 2083–2101.

Oliver, W.C., Pharr, G.M., 1992. An improved technique for determining hardness and elastic-modulus using load and displacement sensing indentation experiments. Journal of Materials Research 7 (6), 1564–1583.

Oliver, W.C., Pharr, G.M., 2004. Measurement of hardness and elastic modulus by instrumented indentation: advances in understanding and refinements to methodology. Journal of Materials Research 19 (1), 3–20.

Pharr, G.M., Oliver, W.C., Brotzen, F.R., 1992. On the generality of relationship among contact stiffness, contact area and elastic modulus during indentation. Journal of Materials Research 7 (3), 613–617.

Seitzman, L.E., 1998. Mechanical properties from instrumented indentation: uncertainties due to tip-shape correction. Journal of Materials Research 13 (10), 2936–2944.

Simo, J.C., Laursen, T.A., 1992. An augmented Lagrangian treatment of contact problems involving friction. Computers & Structures 42 (1), 97–116.

Sneddon, I.N., 1965. The relation between load and penetration in the axisymmetric Boussinesq problem for a punch of arbitrary profile. International Journal of Engineering Science 3, 47–56.

Sun, Y., Bell, T., Zhengs, S., 1995. Finite-element analysis of the critical ratio of coating thickness to indentation depth for coating property measurements by nanoindentation. Thin Solid Films 258 (1–2), 198–204.

Tabor, D., 1951. The Hardness of Metals. Clarendon Press, Oxford.

Thurn, J., Cook, F., 2002. Simplified area function for sharp indenter tips in depth-sensing indentation. Journal of Materials Research 17 (5), 1143–1146.

Trindade, A.C., Cavaleiro, A., Fernandes, J.V., 1994. Estimation of Young's modulus and hardness by ultra-low load hardness tests with a Vickers indenter. Journal of Testing and Evaluation 22 (4), 365–369.